Planetary and Space Science 58 (2010) 279–286

Contents lists available at ScienceDirect

Planetary and Space Science

journal homepage: www.elsevier.com/locate/pss

Magnetic field investigation of Mercury's magnetosphere and the inner heliosphere by MMO/MGF

Wolfgang Baumjohann [a,*], Ayako Matsuoka [b], Werner Magnes [a], Karl-Heinz Glassmeier [c], Rumi Nakamura [a], Helfried Biernat [a], Magda Delva [a], Konrad Schwingenschuh [a], Tielong Zhang [a], Hans-Ulrich Auster [c], Karl-Heinz Fornacon [c], Ingo Richter [c], André Balogh [d], Peter Cargill [d], Chris Carr [d], Michele Dougherty [d], Timothy S. Horbury [d], Elizabeth A. Lucek [d], Fumio Tohyama [e], Takao Takahashi [f], Makoto Tanaka [f], Tsugunobu Nagai [g], Hideo Tsunakawa [g], Masaki Matsushima [g], Hideaki Kawano [h], Akimasa Yoshikawa [h], Hidetoshi Shibuya [i], Tomoko Nakagawa [j], Masahiro Hoshino [k], Yoshimasa Tanaka [l], Ryuho Kataoka [m], Brian J. Anderson [n], Christopher T. Russell [o], Uwe Motschmann [p], Manabu Shinohara [q]

[a] Space Research Institute, Austrian Academy of Sciences, Schmiedlstr. 6, 8042 Graz, Austria
[b] ISAS/JAXA, Yoshinodai, Sagamihara, Kanagawa 229-8510, Japan
[c] Institut für Geophysik und extraterrestrische Physik, Mendelssohnstr. 3, 38106 Braunschweig, Germany
[d] Blackett Laboratory, Imperial College, London SW72AZ, UK
[e] Faculty of Engineering, Tokai University, Hiratsuka, Kanagawa 259-1292, Japan
[f] Information Science Laboratory, Tokai University, Hiratsuka, Kanagawa 259-1292, Japan
[g] Department of Earth and Planetary Sciences, Tokyo Institute of Technology, Meguro, Tokyo 152-8551, Japan
[h] Department of Earth and Planetary Sciences, Kyushu University, Hakozaki, Fukuoka 812-8581, Japan
[i] Department of Earth Sciences, Kumamoto University, Kurokami, Kumamoto 860-8555, Japan
[j] Department of Information and Communication Engineering, Tohoku Institute of Technology, Taihaku, Sendai, Miyagi 982-8577, Japan
[k] Department of Earth and Planetary Science, University of Tokyo, Bunkyo, Tokyo 113-0033, Japan
[l] National Institute of Polar Research, Kaga 1-chome, Itabashi, Tokyo 173-8515, Japan
[m] Computational Astrophysics Laboratory, RIKEN, Hirosawa, Wako, Saitama 351-0198, Japan
[n] Applied Physics Laboratory, Johns Hopkins University, Laurel, MD 20723, USA
[o] Institute of Geophysics and Planetary Physics, University of California, Los Angeles, CA 90024, USA
[p] Institut für theoretische Physik, Mendelssohnstr. 3, 38106 Braunschweig, Germany
[q] Space Environment Research Center, Kyushu University, Hakozaki, Fukuoka 812-8581, Japan

ARTICLE INFO

Article history:
Received 25 February 2008
Received in revised form
17 April 2008
Accepted 16 May 2008
Available online 12 June 2008

Keywords:
Magnetometer
Mercury
Magnetosphere
Inner heliosphere

ABSTRACT

The Mercury magnetospheric orbiter (MMO) of the Japanese–European BepiColombo mission carries a dual-sensor magnetometer, MMO/MGF. The sensors are of the classical fluxgate type mounted on a boom. For redundancy, each sensor carries its own electronics and is connected to a different data processing unit. MMO/MGF can sample the magnetic field at a rate of up to 128 Hz. The resulting comparatively high time resolution of the magnetic field measurements, i.e., down to 8 ms, will be necessary when studying the dynamics of and processes within the Hermean magnetosphere, since the Mariner 10 observations have shown that their typical time scales are much shorter than in the Earth's magnetosphere, by about a factor of 30. The high time resolution will also be very useful for studying the evolution of the still young solar wind plasma as well as interplanetary shocks at 0.3–0.46 AU. Of course, MMO/MGF is also well-prepared to assist the sister magnetometer aboard the Mercury planetary orbiter, MPO/MAG, in measuring Mercury's intrinsic magnetic field, in particular by helping to distinguish between temporal fluctuations and spatial variations.

1. Introduction

The discovery of Mercury's planetary magnetic field by the Mariner 10 mission more than 30 years ago was likely the most surprising result of that mission, one that had important consequences for understanding the origin, evolution, and present state of the Mercury's interior (e.g., Balogh, 1997). Prior to Mariner 10, Mercury had been thought to have a completely solid iron core. An important consequence of Mercury's planetary magnetic field is the existence of a planetary magnetosphere, resulting, as in the case of the Earth, from the interaction of the solar wind with the planetary magnetic field. However, the small size of the

* Corresponding author.
E-mail address: baumjohann@oeaw.ac.at (W. Baumjohann).

0032-0633/$ - see front matter © 2009 Elsevier Ltd. All rights reserved.
doi:10.1016/j.pss.2008.05.019

magnetosphere and its dynamics lead to much shorter response and transit times than at the Earth. Understanding the magnetosphere of Mercury is important both for its own sake as well as in comparison with those known from other examples (Earth, Jupiter, and Saturn). Furthermore, any spacecraft orbiting Mercury will spend long times in the still young and evolving solar wind and may observe interplanetary shock waves at still high Mach numbers, thus allowing heliospheric studies with modern instrumentation in a parameter regime hitherto observed 20–30 years ago by the Helios spacecraft.

2. Key science issues

In the following, we shortly list the key science topics to be addressed by using Mercury magnetospheric orbiter, MMO/MAG data; a more extensive description can be found in Baumjohann et al. (2006).

2.1. Magnetosphere

Mercury's magnetosphere is unique due to its modest intrinsic magnetic field, lack of an ionosphere, and closeness to the Sun. Its magnetic field is sufficiently strong to stand off the solar wind above the surface under most conditions, but it is weak to the point where the planet itself occupies most of the forward magnetosphere. The small size of the Hermean magnetosphere implies that kinetic effects become very important for most magnetospheric processes, as the typical scales of the magnetosphere are of the order of a few to a few tens of ion gyro radii.

In summary, the small dimension of the Hermean magnetosphere, the fast transit times, the importance of kinetic effects on larger scales, the lack of an ionosphere, and the strong forcing by the 'young' solar wind, all interrelated, make up a magnetosphere which might be quite different from that of the Earth, yet the Mariner 10 observations showed phenomena similar to those operating in the terrestrial magnetosphere. The key difference was that typical processes in the Hermean magnetosphere occur much faster, by about a factor of 30, than at Earth (see Table 1), mainly due to shorter transit times in the much smaller magnetosphere (Table 2).

This factor-of-thirty is the key design driver for the magnetometer on board MMO. Measurements need to be taken at a much faster rate than typically done in the Earth's magnetosphere. Hence, MMO/MGF will use a 128 Hz sampling rate. Magnetometers with such a sampling rate have been flown on Equator-S (Fornacon et al., 1999) in the terrestrial magnetosphere and are presently in orbit around Venus and Earth aboard the Venus Express (Zhang et al., 2006) and THEMIS (Auster et al., 2008) space probes, respectively. In particular, the Equator-S measurements have shown the usefulness of extending the DC magnetometer frequency range up to 64 Hz (e.g., Baumjohann et al., 1999a, b, 2000; Lucek et al., 2001).

Using MMO/MGF data, three main topics of interest in magnetospheric physics will be addressed:

Reconnection is the first topic. Magnetic reconnection is a key process in the energization of all intrinsic magnetospheres explored to date. There are many outstanding questions on magnetic reconnection between the interplanetary magnetic field (IMF) and Mercury's intrinsic magnetic field. Substorm-like events in the Mariner 10 observations (Siscoe et al., 1975) clearly show that magnetic reconnection takes place. The Hermean magnetosphere provides us a unique setting in which to examine problems ubiquitous in magnetized plasmas, the resulting knowledge from which can be applied to better understanding their terrestrial analogues. On the dayside, the conditions in the solar wind plasma may increase the rate of reconnection at Mercury, because the plasma beta is smaller at 0.39 AU than at 1 AU. At Earth, smaller beta leads to higher Alfvén velocities and higher reconnection rates (e.g., Paschmann et al., 1986). On the nightside, the lack of an atmosphere and thus a likely smaller mass density in the Hermean magnetotail because of lower supply may increase the reconnection rate there, too.

Field-aligned currents are a natural second topic. The terrestrial magnetosphere is tightly coupled to the Earth's ionosphere by field-aligned currents that flow along the magnetic lines of force and close via Pedersen and Hall currents in the terrestrial ionosphere. At Mercury, Slavin et al. (1997) reported magnetic field perturbations that are strongly suggestive of field-aligned currents, but it is unclear how these currents are closed in the absence of an ionosphere. It is presently unknown whether the field-aligned currents are closed through the only weakly conducting surface regolith or via plasma currents within the magnetosphere itself (Glassmeier, 2000). Furthermore, Joule heating in the ionosphere due to field-aligned current-fed Pedersen currents is a major dissipation process for magnetospheric dynamics in the terrestrial case. If this dissipation mechanism is much weaker at Mercury, magnetosphere–ionosphere coupling processes as well as energy budgets may be quite different in the Hermean magnetosphere.

Last but not the least, low-frequency waves will be studied. Ultra-low frequency (ULF) waves at the Earth can mostly be understood using a magnetohydrodynamic description of the plasma. At Mercury the existence of ULF waves has been demonstrated by, e.g., Fairfield and Behannon (1976) and Russell (1989). But conditions at Mercury are very different as the magnetospheric scale is rather small and comparable to the thermal ion gyro radius (e.g., Othmer et al., 1999; Glassmeier, 2000). This implies that kinetic effects will play a major role for the generation and propagation of ULF waves (Glassmeier et al., 2004). Other low-frequency waves are, of course, also of interest (see, e.g., Blomberg et al., 2007).

Table 1
Typical time scales in the Hermean and terrestrial magnetosphere.

Process	Mercury	Earth (min)
Tail response	1 min	20
Substorm	1–2 min	30–60
Alfvén travel time	5–10 s	2
Flux transfer event	2 s	1

Table 2
Summary of resource requirements.

Mass	MGF-OE PCB with mounting frame	188 g
	MGF-IE PCB with mounting frame	358 g
	MGF-OS w/o harness and thermal H/W	100 g
	MGF-IS w/o harness and thermal H/W	120 g
	Total MGF instrument mass	766 g
Power	MGF-O	1.65 W
	MGF-I	2.78 W
	Total MGF operating power	4.43 W
Telemetry	High	7700 bit/s
	Medium	420 bit/s
	Low	62 bit/s
	Checkout	15,400 bit/s

2.2. Inner heliosphere

The inner heliosphere between 0.3 and 0.5 AU is known from Helios observations in the 1970s to be quite different from that

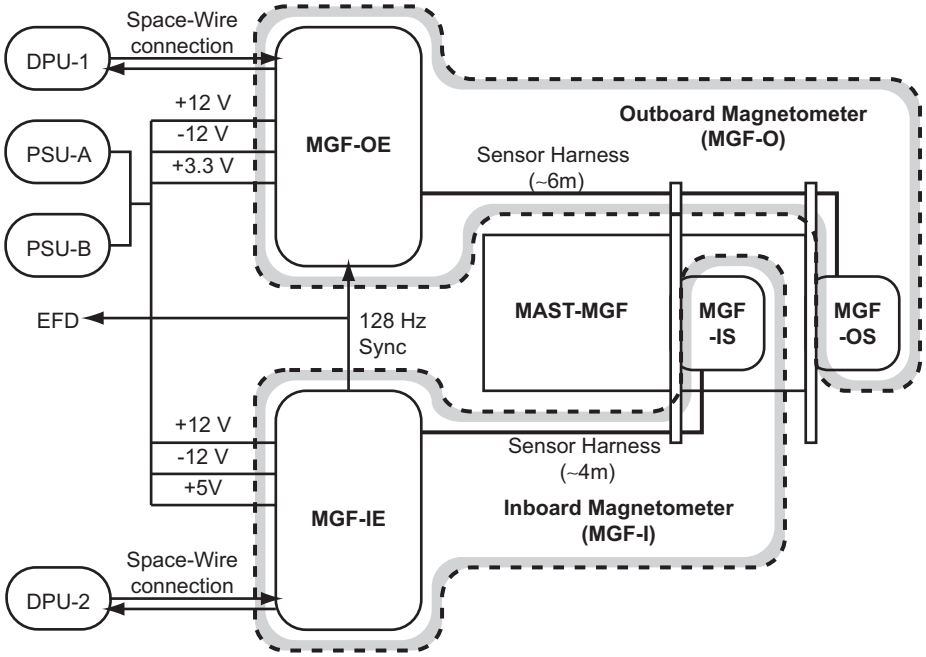

Fig. 1. Block diagram of the MGF magnetometer.

around 1 AU. Since MMO will spend considerable time in the solar wind, it will be possible to study this parameter regime with more modern instruments. In particular, magnetic field observations with high temporal resolution will help to clarify the role of magnetic fluctuations in solar wind heating and acceleration. It is expected that the MMO/MGF observations will be crucial to help understandthe interplay between ion cyclotron resonances and linearly polarized Alfvén waves (e.g., Hollweg and Isenberg, 2002; Suzuki, 2002).

As a second topic, interplanetary shocks in the inner heliosphere and the Hermean bow shock itself can be examples of very high and very low Mach number shocks, respectively, where the physics involved is likely different from that observed at shocks further out in the solar system. Since the solar wind speed at Mercury's orbit is almost the same as at Earth, but the magnitude of the IMF is increased about five times and density by close to a factor of ten, the Mach number of the Hermean bow shock is lower than that of the Earth's bow shock, and for extreme conditions it could be less than unity, i.e., turn from a fast shock into an intermediate or even a slow shock. On the other hand, for interplanetary shocks initiated by solar flares, very high Mach number shocks might be observed at Mercury's orbit during the solar maximum phase. From compound studies of observations and modeling (Smart and Shea, 1985; Cliver et al., 1990), Alfvénic Mach numbers are known to reach up to several tens for the strongest interplanetary shocks. Hence, high Mach number shock observations at Mercury's orbit could provide an important clue to bridge the gap of our understanding of the superhigh Mach number astrophysical shocks and high Mach number shocks seen in heliosphere, especially the relative heating of electrons and ions (see, for example, Cargill and Papadopoulos, 1988; Hoshino and Shimada, 2002).

3. Instrument description

The MMO/MGF instrument is composed of two separate tri-axial fluxgate magnetometers: outboard (MGF-O) and inboard magnetometer (MGF-I). The overall MGF instrument design (without housekeeping measurements) is depicted in Fig. 1. The outboard sensor (MGF-OS) is mounted to the tip of a 4.4-m-long boom (MAST-MGF) designed for the mounting of the fluxgate sensors. The inboard sensor (MGF-IS) is mounted at 1.6 m distance from the boom's tip. Both sensors are connected to their dedicated sensor electronics (MGF-OE and MGF-IE) via a several-metres long sensor harness. Using two sensors in a gradiometer configuration allows applying the so-called *dual-magnetometer* technique (e.g., Ness et al., 1971; Hedgecock, 1975; Georgescu et al., 2008) for a proper determination of magnetic stray fields caused by magnets and currents in the S/C body.

Both magnetometers have a dynamic range of ± 2000 nT and transmit raw data with a 128 Hz vector rate and 20 bit digital resolution (3.8 pT) to the data-processing units (DPUs). Each sensor has its own sensor electronics board (208×148 mm^2). It provides the excitation and feedback currents to the fluxgate sensor and detects and processes the field-related signals from the pick-up coils. The two boards are connected to different power supplies. The electronics boards are connected to separate DPUs (MGF-OE to DPU-1 and MGF-IE to DPU-2), which are located in a different electronics box, and the same fully redundant power supply unit (PSU). The MGF electronics is supplied by three voltages (MGF-OE: ± 12 and +3.3 V; MGF-IE: ± 12 and +5 V) and the electronics are connected to the DPUs via Space Wire, a standard protocol used in spacecraft to interconnect digital systems.

Since MGF-O and MGF-I will be operated from different master clocks, it is necessary to synchronize them. For this reason, a 128 Hz sync-signal is provided by MGF-I to MGF-O (as well as to the electric field instrument, EFD) through low-voltage differential signal (LVDS) drivers which enable the generation of fully synchronous vector pairs.

With the MGF design, redundancy for the magnetic field measurement is implemented to the highest possible degree. The two independent magnetometers MGF-O and MGF-I are connected to two separate DPUs and the power supply is guaranteed by two fully redundant PSUs; also, their instrument designs (electronics and sensors) are completely different, so that a total failure of the magnetic field investigation aboard MMO is very unlikely.

3.1. Outboard magnetometer MGF-O

The MGF-O magnetometer is designed and manufactured in a joint effort by the Space Research Institute (Institut für Weltraumforschung (IWF)) of the Austrian Academy of Sciences and the Institut für Geophysik und extraterrestrische Physik (IGEP) of the Technical University in Braunschweig, Germany. The MGF-O sensor electronics is mainly subcontracted to Magson GmbH, Germany, and the instrument calibration is supported by Imperial College in London.

The magnetometer is based on the so-called digital magnetometer design (Auster et al., 1995). This sensor electronics concept reduces the amount of analogue parts by digitizing the output signal of the pick-up coil directly after the input amplifier at a sampling frequency which is four times the excitation frequency. The traditional analogue signal processing is replaced by mathematical algorithms implemented in a field programmable gate array (FPGA) which also handles the serial interface to the common DPU. The digital magnetometer was first developed for ESA's Rosetta Lander mission (Auster et al., 2007). In further miniaturized configurations it is also realized in VEXMAG aboard Venus Express (Zhang et al., 2006, 2007) and FGM aboard THEMIS (Auster et al., 2008).

The MGF-O sensor consists of the sensor core and a stand-off made from PEEK, which improves the thermal de-coupling of the sensor core from the MAST interface (see Fig. 2). Two entwined ring-cores with diameters of 13 and 18 mm, respectively, are used for measuring the magnetic field in a vector-compensated sensor set-up. Via the smaller ring-core the magnetic field is measured in *X* and *Z* directions, while the larger is used for *Y* and *Z*. The ring-cores are equipped with two 3D coil systems: an inner one to collect (pick up) the magnetic field-dependant second harmonic of the fundamental excitation frequency and an outer Helmholtz coil system to compensate for the external field at the ring-core position. The pick-up coil system is attached as close as possible to the ring-cores to increase the signal-to-noise ratio. It is in contrast to the comparably much larger Helmholtz coils which are used as a feedback system to homogenously compensate the magnetic field vector at the core position. The vector compensation keeps the sensitive sensor element in zero field, which has the advantage that besides the scale value also the orientation of the field axes is only dependant on the mechanically well-stabilized feedback coils. All coils are made from bond-coated copper wire. By using this technology, additional mechanical support, e.g. ceramic rings, can be reduced to a minimum. Furthermore, the combination of materials with different thermal expansion coefficients can be avoided and mass can be saved. As a result, the mass of the sensor core (excluding harness, mounting elements, protection cap, and thermal hardware) could be reduced to less than 40 g for the type of sensor used for MGF-O. The height and diameter of the cylindrically shaped envelope of the sensor core are about 91 and 55 mm, respectively.

In order to survive the harsh temperature conditions in the orbit around Mercury, all sensor parts, including the circular printed circuit board and the parallel capacitor needed for a proper current peak driven through the excitation coil, are selected and qualified for a maximum operating temperature of 200 °C. Both MGF-OS and MGF-IS have already undergone this testing and proved to operate flawlessly between −60 and 200 °C.

The block diagram of the MGF-O sensor electronics is shown in Fig. 3. It generates an AC excitation current (excitation frequency of 9600 Hz, F0), which drives the soft–magnetic core material (13Fe–81Ni–6Mo alloy) of two ring-cores deeply into positive and negative saturation. The external magnetic field distorts the symmetry of the magnetic flux and generates field proportional even harmonics of the excitation frequency in the pick-up coils.

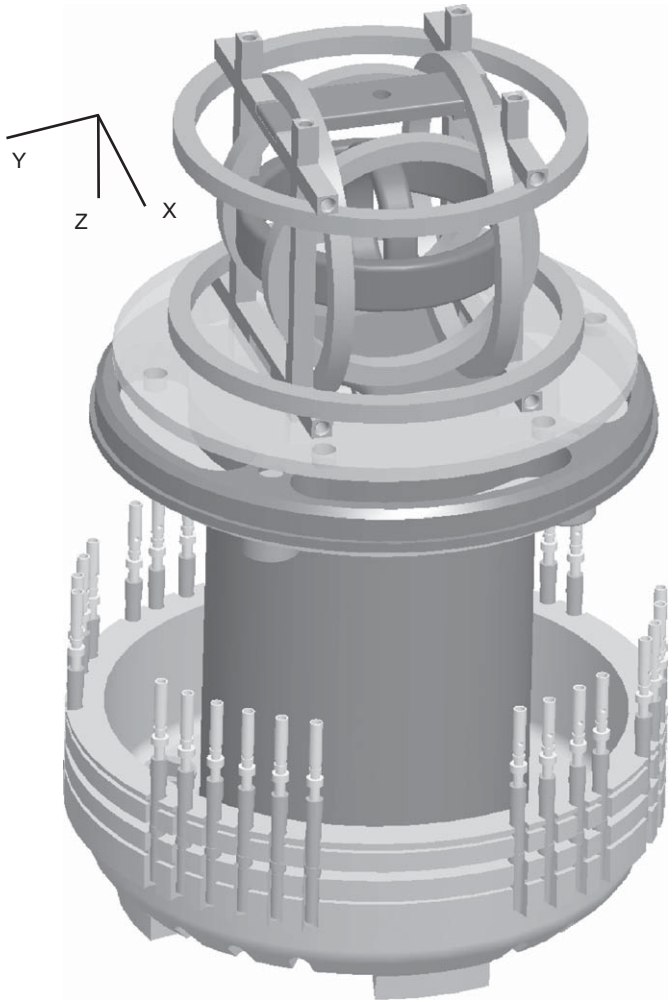

Fig. 2. 3-D model of MGF-OS.

The induced voltage in the pick-up coils is digitized after the preamplifier at a sampling frequency which is four times the excitation frequency. The accumulation of multiples of four consecutive data samples is necessary in order to cancel out all odd harmonics of the excitation signal, which couple from the excitation to the pick-up coil inductively. After processing the magnetic field digitally, the feedback settings are updated so that the field generated by the Helmholtz coil system compensates the external field almost completely.

The overall instrument performance is widely influenced by the sensor interface electronics. 14-bit analogue-to-digital converter (ADCs, Maxwell 7872) and 16-bit digital-to-analogue converter (DACs, MAX542) are used for the described design. The digital resolution of the 14-bit ADC at an input voltage range of ± 5 V is 0.6 mV, with a theoretically white quantization noise of 0.173 mV_{RMS}. Considering a ratio of 300 between sampling (4F0, 38.4 kHz) and maximum output frequency (128 Hz), the quantization noise in the signal bandwidth is 10 μV_{RMS}. With a nominal sensor sensitivity of 0.005 mV/nT and a preamplification of 40 dB (limited by additional odd harmonics in the pick-up signal), the amplitude of the digitization error is in the order of 20 pT_{RMS} for a signal bandwidth of 64 Hz. It corresponds to a noise density of less than 3 pT/sqrt(Hz), when assuming a white noise behavior, which is acceptable for this application.

More critical is the limitation of the DAC performance and here especially the nonlinearity, which is traditionally in the order of

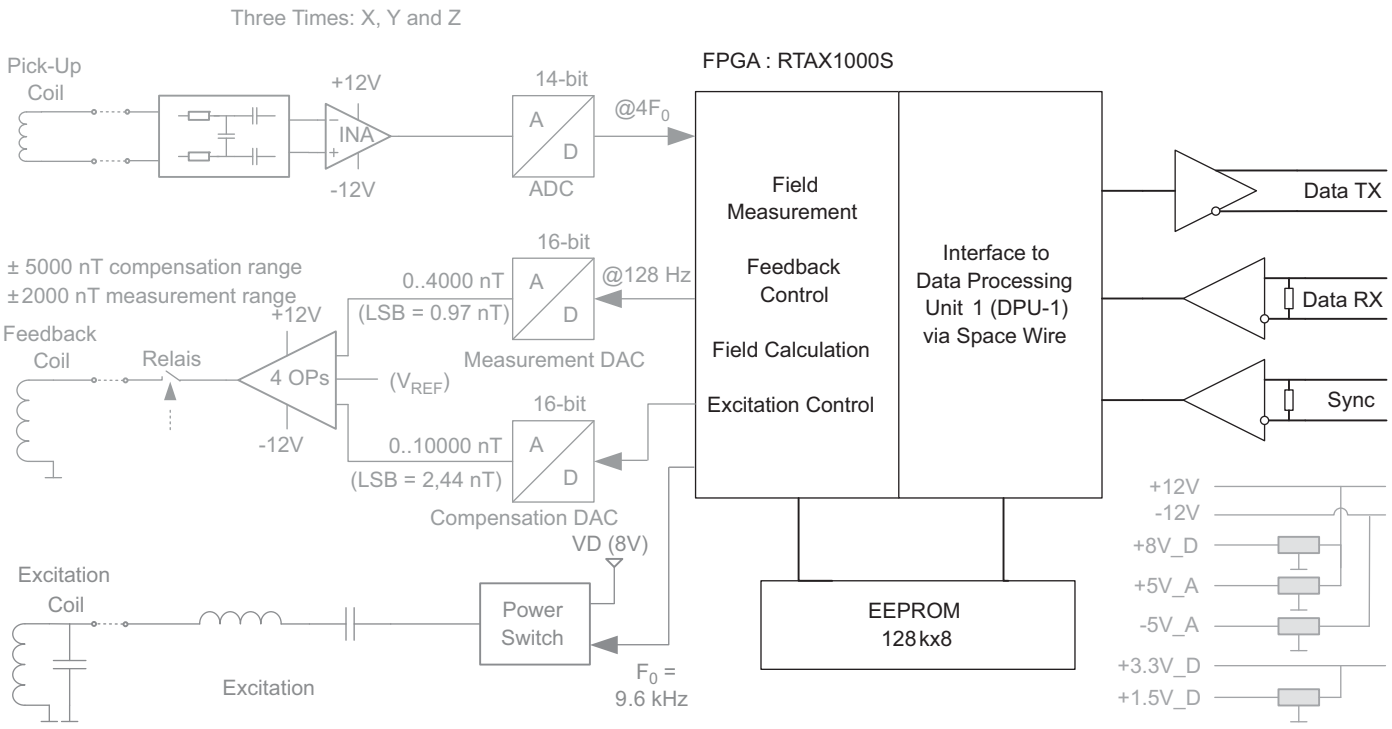

Fig. 3. Block diagram of MGF-O magnetometer.

one quarter of the least significant bit. This is why a 16-bit DAC (MAX542) is used for MGF-O (instead of 12-bit DACs used for all the missions before). Since a nulling feedback field increases the overall linearity and stability of the measurement, it is applied to all sensor elements via one feedback/measurement DAC and a separate pair of feedback coils per sensor axis. For the measurement range of ± 2000 nT, a maximum linearity error of about 15 pT is expected. Additionally, an artificial magnetic field of ± 5000 nT can independently be applied to each sensor component via a second 16-bit DAC per channel for compensation of unexpected DC stray fields which are bigger than the measurement range. This feature is mainly required for instrument checkout during cruise phase when the MAST is still in its stored position or in case of a deployment failure and when science operation must be performed in an un-deployed configuration.

The core of the digital fluxgate electronics is an RTAX1000S FPGA from Actel. Its functionality can be divided into three sections: interface to sensor and MGF-I (receipt of sync signal), interface to EEPROM (program load) and DPU via SpaceWire (SpW) and a 32-bit RISC processor module especially developed for the THEMIS magnetometer.

The sensor interface enables the excitation; it starts the ADC sampling with programmable phase shift versus excitation clock at all three channels synchronously, averages (sign sensitive) a programmable number of ADC values, and sends the results to the processor module. The processor calculates the magnetic field vector by adding the old DAC and new ADC values, both scaled by programmable conversion factors $k1$ and $k2$. Additionally, new feedback settings are calculated and passed to the sensor interface. High-resolution 128 Hz data, containing the magnetic field vector (3×20 bit word) and status information, are continuously transferred via output registers to the Space Wire interface, which also handles the receipt of commands for configuring hardware and software. The MGF-O raw data are synchronized to the field acquisition in the MGF-I instrument via a 128 Hz synchronization clock provided by MGF-I.

3.2. Inboard magnetometer MGF-I

The MGF-I magnetometer is designed and manufactured by ISAS/JAXA. It is a conventional *analogue* fluxgate-type magnetometer. It is very similar to those used aboard previous Japanese space missions, e.g., Akebono (Fukunishi et al., 1990), Geotail (Kokubun et al., 1994), and Nozomi (Yamamoto and Matsuoka, 1998). In the case of an analogue magnetometer, the second-harmonic component of the pickup signal is detected, rectified, and integrated by analogue circuits. An ADC digitizes the intensity of the cancellation current of the external field, which is linearly related to the external field.

The MGF-IS sensor measures the orthogonal tri-axial magnetic fields with an identical ring-core type single-sensor for each axis. A single-sensor consists of driving and combined pickup/feedback parts. The driving part contains a 20 mm ring-core of nickel–molybdenum Permalloy and a coil wound along the circumference. The pickup/feedback part consists of another coil and a parallelepiped ceramic bobbin circumscribing the driving part. The three single sensors are put together in a sensor unit on a ceramic stand as presented in Fig. 4. A carbon fibre re-enforced plastics (CFRP) box covers the sensor unit to protect the sensor component. The driving coils of three sensor components are serially connected to the driving circuit via a twist-pair cable. The driving circuit generates a 11 kHz pulse current of 600 mA peak-to-peak. The amplitude of the driving current is optimized to reduce the power consumption and to enable stable performance in the wide temperature range. The averaged power consumption in the sensor unit is 142 mW.

The block diagram of the MGF-I sensor electronics is shown in Fig. 5. The 11 kHz control signal for the drive/excitation circuit is generated by FPGA–MSP (RTSX72SU from Actel) from the master clock generated by a 8 MHz crystal. The drive circuit excites an AC current at 11 kHz in the coil wound around the ring-core. The electronics preamplifiers amplify the signal induced in the combined pickup/feedback coil. The preamplifier also has the

function of a band-pass filter and effectively amplifies the 22 kHz signal, which is the second harmonics of the drive frequency. The synchronous detectors rectify the second harmonic signal. The output signal of the rectifier is integrated to supply the cancellation current in the pick-up/feedback coil. To reduce the power consumption, a single-power supply, rail-to-rail type OP-AMP (OP484) is used for the preamplifiers and the delta–sigma analogue-to-digital conversion (ADC).

MGF-I has a single dynamic range of ± 2000 nT and a digital resolution of 20 bit (3.8 pT). It allows high-resolution magnetic field measurement even in strong fields. It is realized by 20-bit ADC. Although there are popular commercial ADC ICs of 20-bit resolution or higher, their reliability in the high radiation environment around Mercury has not been established yet. Hence, a delta–sigma ADC circuit has been developed to satisfy the 20-bit resolution, 128 Hz sampling, and tolerance for the radiation environment at Mercury. Fig. 6 shows the block diagram of the delta–sigma ADC design for MGF-I. It consists of an analogue delta–sigma modulation circuit made from a 14-bit ADC and a 12-bit DAC as well as a finite impulse response (FIR) filter in the FPGA-MSP. The delta–sigma modulator generates raw data with 16 kHz as the output of 14-bit ADC. The modulated data are fed back to the DAC and subtracted from the next input data value. The FPGA filters the digitized data and outputs the 128 Hz digital data with 20 bit resolution. FPGA–SpW (again RTSX72SU) handles the digital interface between sensor electronics and DPU-2.

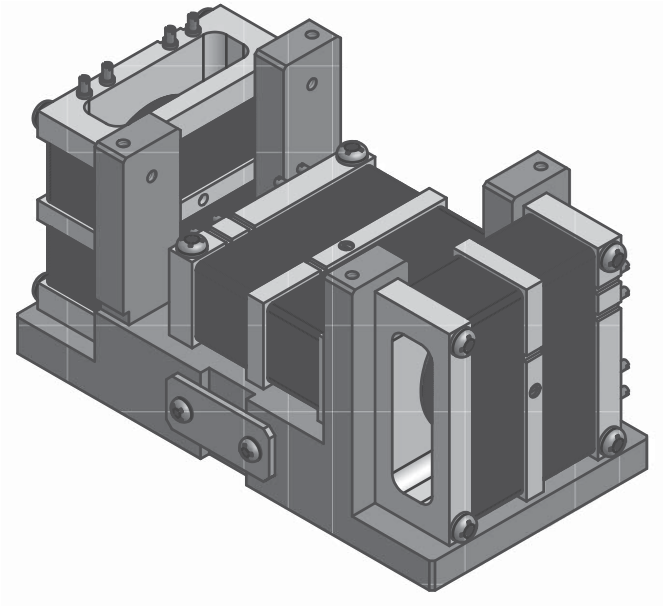

Fig. 4. Tri-axial sensor unit of MGF-IS.

4. Calibration

Many parameters will be determined on the ground before installation of the magnetometer on the spacecraft. Calibration facilities such as magnetic shielding containers (some with controlled temperature) and geomagnetic field cancellation coils are available at ISAS/JAXA in Japan, at the Space Research Institute in Graz (Austria), and the Technical University Braunschweig (Germany). Scale factor and sensor alignment of the two magnetometers, MGF-O and MGF-I, will be evaluated simultaneously at one single facility to check for consistency.

In the preliminary thermal model, the sensor temperatures are estimated to range from -26 to 165 °C for MGF-O and from 16 to 186 °C for MGF-I during the scientific observation phase. The dependence of the offset, scale factor, orthogonality, and noise on the sensor temperature will be examined in a wide temperature range, covering the estimates for the observation phase with adequate margin.

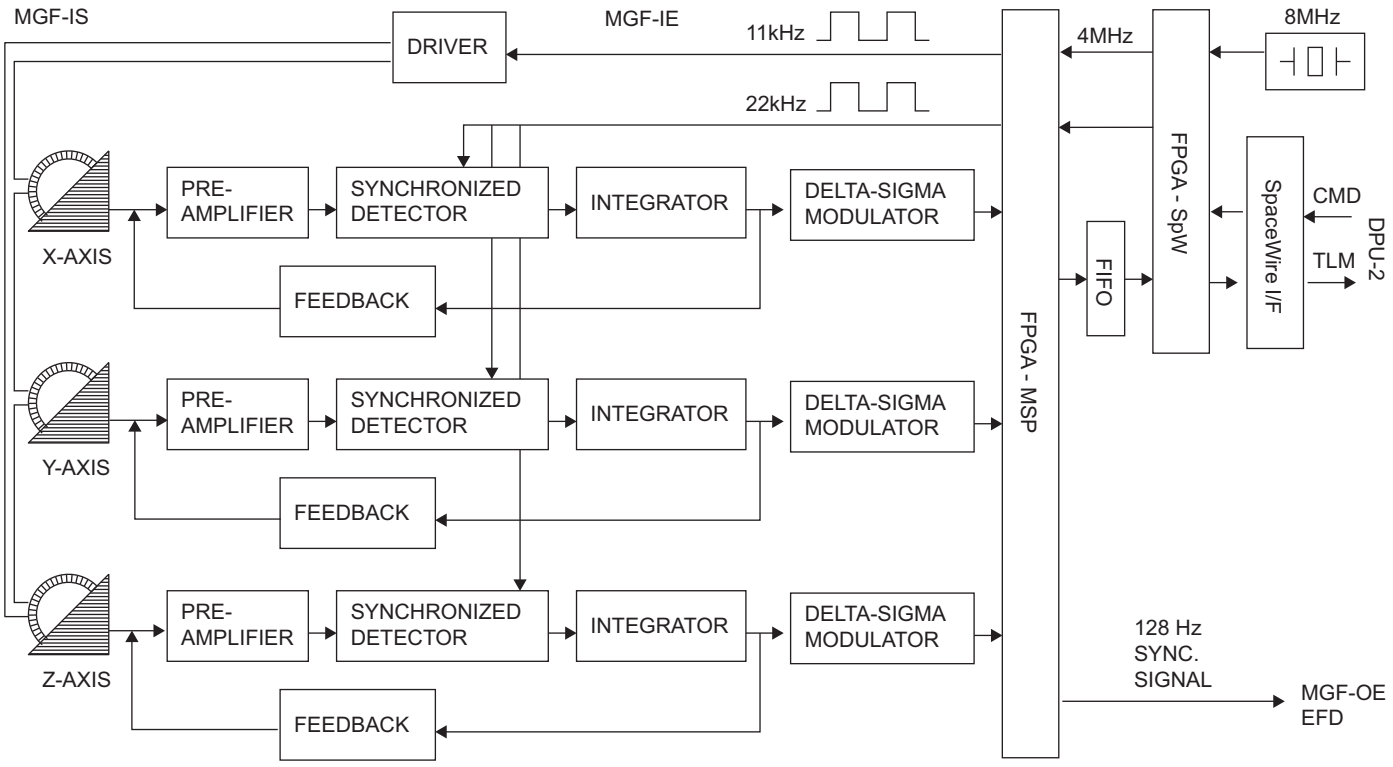

Fig. 5. Block diagram of the MGF-I magnetometer.

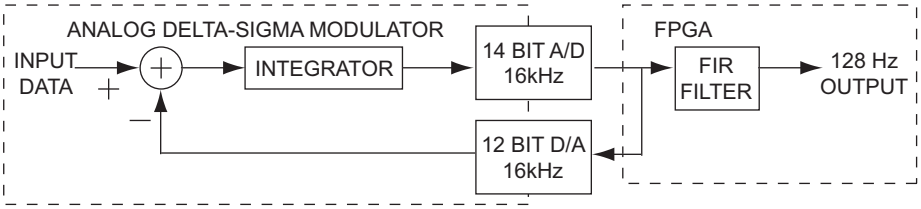

Fig. 6. Block diagram of the delta–sigma analogue-to-digital converter.

There are two types of parameters which are determined directly from the in-flight data. One is the offset (mixture of contributions from the magnetometer and spacecraft stray fields) in the spacecraft spin plane. The other is the sensor inclination angle off the spin plane and the sensor rotation angle around the boom axis. These parameters will be determined during periods of relatively stable background magnetic field. The offset in the direction of the spin axis can be quantified using the characteristics of Alfven waves in the solar wind, which MMO will encounter once every revolution around Mercury. There is no method to determine the sensor azimuth angle, but the error is guaranteed to be within 0.5° if the boom is extended normally.

5. Data products

MGF-O and MGF-I each produce three 20-bit data streams corresponding to the three orthogonal axes at 128 Hz sampling rate. The data are provided to other instruments on board to inform these instruments about magnetic field direction and intensity. The same DPU which sends commands to MGF-O or MGF-I will collect the data from the two sensors and process them. Each DPU reduces the data volume to meet the telemetry budget assigned to MGF. At first 16 effective bits are selected from the 20 bits so that the one-digit resolution varies from 4 to 62 pT, depending on the field intensity. Since the field intensity is estimated to be less than 200 nT at the MMO orbit except for unusual events (e.g., interplanetary shocks in the solar wind), the typical resolution may be expected to be 8 pT or better most of the time. In a second step, the data rate is reduced by averaging and the vector is converted into coordinates fixed to the rest frame.

There are three observational telemetry modes and a CHECKOUT mode. In all modes except CHECKOUT, the data production rate of the primary sensor (the one with the higher accuracy and less interference from the spacecraft stray fields) is higher than that of the other sensor. At present we assume that MGF-O will be the primary sensor. HIGH is the mode for selected events where high-time resolution data are important. The data rate of MGF-O is the same (128 Hz) as that of the original sampling. During the commissioning phase and for a few months at the beginning of the science observation phase, the MGF-I data rate in HIGH mode will be 32 Hz to detect any magnetic interference from the satellite. After the commissioning phase the MGF-I data rate will be reduced to 8 Hz. MEDIUM is the mode for normal operation and LOW is the mode for solar wind monitoring. In these two modes the MGF-O data rate will be 8 and 1 Hz and 16 or 8 times higher, respectively, than that of MGF-I. The status of MGF (sensor temperature, electronics board temperature, FPGA processing status) is monitored every 8 s. The CHECKOUT mode is meant for a full-health check of the instrument. In this mode, the original 20 bit data are transmitted to the ground at 128 Hz with 1 Hz status data. The final definition of the modes and the telemetry budget will be determined in the discussion by the Science Operation Working Group.

6. Collaboration with other instruments

Naturally, only some of the aforementioned research topics (mainly field-aligned currents and ULF waves) will be solved by using the MMO/MGF data alone. While the magnetometer data will be key to understanding these phenomena, it will often be beneficial, if not essential, to include data from other instruments.

As in many space plasma physics studies, looking simultaneously into the ion plasma and magnetic field data will suffice to answer many questions. Hence, close collaboration with the mercury plasma particle experiment (MPPE) aboard MMO (Saito et al., 2008) is foreseen when studying the inner heliosphere, reconnection processes, and especially Hermean solar wind–-magnetosphere coupling (see, e.g., Fujimoto et al., 2007) and magnetospheric particle acceleration processes (see, e.g., Zelenyi et al., 2007) can only be solved by using data simultaneously taken by MPPE and MGF data. Furthermore, studies of low-frequency waves in the tens-of-Hz range, in solar wind and magnetosphere, will surely benefit from simultaneous measurements by the magnetometer and the MMO plasma wave package (Kasaba et al., 2008).

While MPO is primarily a planetary orbiter with many remote sensing instruments, two of its instrument packages offer opportunities for two-spacecraft studies of the Hermean plasma environment (see Milillo et al., 2008): the magnetometer MPO/MAG (Glassmeier et al., 2008) and the SERENA suite of four particle instruments (ELENA, STROFIO, PICAM, and MIPA) (Orsini et al., 2008). Moreover, MMO/MGF will assist MPO/MAG in studying the internal magnetic field of Mercury by making it possible, or at least more easy, to distinguish between the static internal and the variable external contribution to the measured magnetic field.

References

Auster, H.U., Lichopoj, A., Rustenbach, J., Bitterlich, H., Fornacon, K.H., Hillenmaier, O., Krause, R., Schenk, H.J., Auster, V., 1995. Concept and first results of a digital fluxgate magnetometer. Meas. Sci. Technol. 5, 477–481.

Auster, H.U., Apathy, I., Berghofer, G., Remizov, A., Roll, R., Fornacon, K.H., Glassmeier, K.H., Haerendel, G., Hejja, I., Kührt, E., Magnes, W., Moehlmann, D., Motschmann, U., Richter, I., Rosenbauer, H., Russell, C.T., Rustenbach, J., Sauer, K., Schwingenschuh, I., Szemerey, K., Waesch, R., 2007. ROMAP: Rosetta magnetometer and plasma monitor. Space Sci. Rev. 128, 221–240.

Auster, H.U., Glassmeier, K.H., Magnes, W., Aydogar, O., Baumjohann, W., Constantinescu, D., Fischer, D., Fornacon, K.H., Georgescu, E., Harvey, P., Hillenmaier, O., Kroth, R., Ludlam, M., Narita, Y., Nakamura, R., Okrafka, K., Plaschke, F., Richter, I., Schwarzl, H., Stoll, B., Valavanoglou, A., Wiedemann, M., 2008. The THEMIS fluxgate magnetometer. Space Sci. Rev., in press.

Balogh, A., 1997. Mercury, the planet and its magnetosphere. Planet. Space Sci. 45, 1–2.

Baumjohann, W., Haerendel, G., Treumann, R.A., Bauer, T., Rustenbach, J., Georgescu, E., Auster, U., Fornacon, K.-H., Glaßmeier, K.-H., Lühr, H., Büchner, J., Nikutowski, B., Balogh, A., Cowley, S.W.H., 1999a. First ELF wave measurements with the Equator-S magnetometer. Adv. Space Res. 24, 77–80.

Baumjohann, W., Treumann, R.A., Georgescu, E., Haerendel, G., Fornacon, K.-H., Auster, H.U., 1999b. Waveform and packet structure of lion roars. Ann. Geophys. 17, 1528–1534.

Baumjohann, W., Georgescu, E., Fornacon, K.-H., Auster, H.U., Treumann, R.A., Haerendel, G., 2000. Magnetospheric lion roars. Ann. Geophys. 18, 406–410.

Baumjohann, W., Matsuoka, A., Glassmeier, K.-H., Russell, C.T., Nagai, T., Hoshino, M., Nakagawa, T., Balogh, A., Slavin, J.A., Nakamura, R., Magnes, W., 2006. The

magnetosphere of Mercury and its solar wind environment: open issues and scientific questions. Adv. Space Res. 38, 604–609.
Blomberg, L.G., Cumnock, J.A., Glassmeier, K.-H., Treumann, R.A., 2007. Plasma waves in the Hermean magnetosphere. Space Sci. Rev. 132, 575–591.
Cargill, P.J., Papadopoulos, K., 1988. A mechanism for strong electron heating at shocks in supernova remnants. Astrophys. J. Lett. 329, L29–L32.
Cliver, E.W., Feynman, J., Garrnett, H.B., 1990. An estimate of the maximum speed of the solar wind 1988–1989. J. Geophys. Res. 95, 17103–17112.
Fairfield, D.H., Behannon, K.W., 1976. Bow shock and magnetosheath waves at Mercury. J. Geophys. Res. 81, 3897–3906.
Fornacon, K.-H., Auster, H.U., Georgescu, E., Baumjohann, W., Glassmeier, K.-H., Rustenbach, J., Dunlop, M., 1999. The magnetic field experiment onboard Equator-S and its scientific possibilities. Ann. Geophys. 17, 1521–1527.
Fujimoto, M., Baumjohann, W., Kabin, K., Nakamura, R., Slavin, J.A., Terada, N., Zelenyi, L., 2007. Hermean magnetosphere—solar wind interaction. Space Sci. Rev. 132, 529–550.
Fukunishi, H., Fujii, R., Kokubun, S., Hayashi, K., Tohyama, F., Tonegawa, Y., Okano, S., Sugiura, M., Yumoto, K., Aoyama, I., Sakurai, T., Saito, T., Iijima, T., Nishida, A., Natori, M., 1990. Magnetic field observations on the AKEBONO (EXOS-D) satellite. J. Geomagn. Geoelectr. 42, 385–409.
Georgescu, E., Auster, H.U., Takada, T., Gloag, J., Eichelberger, H., Fornaçon, K-H., Brown, P., Carr, C.M., Zhang, T.L., 2008. Modified gradiometer technique applied to Double Star (TC-1). Adv. Space Res.
Glassmeier, K.-H., 2000. Currents in Mercury's magnetosphere. In: Magnetospheric Current Systems, Geophys. Monograph 118. AGU, pp. 371–383.
Glassmeier, K.-H., Klimushkin, D., Othmer, C., Mager, P., 2004. ULF waves at Mercury: earth, the giants and their little brother compared. Adv. Space Res. 33, 1875–1883.
Glassmeier, K.-H., Auster, H.U., Heyner, D., Okrafka, K., Carr, C., Berghofer, G., Anderson, B.J., Balogh, A., Baumjohann, W., Cargill, P.J., Christensen, U., Delva, M., Dougherty, M., Fornacon, K.H., Horbury, T.S., Lucek, E.A., Magnes, W., Mandea, M., Matsuoka, A., Matsushima, M., Motschmann, U., Nakamura, R., Narita, Y., Richter, I., Schwingenschuh, K., Shibuya, H., Slavin, J.A., Sotin, C., Stoll, B., Tsunakawa, H., Vennerstrom, S., Vogt, J., Zhang, T.L., 2008. The fluxgate magnetometer of the BepiColombo planetary orbiter. Planet. Space Sci. 56, 287–299.
Hedgecock, P.C., 1975. A correlation technique for magnetometer zero level determination. Space Sci. Instrum. 1, 83–90.
Hollweg, J.V., Isenberg, P.A., 2002. Generation of the fast solar wind: a review with emphasis on the resonant cyclotron interaction. J. Geophys. Res. 107, 1147.
Hoshino, M., Shimada, N., 2002. Nonthermal electrons at high Mach number shocks: electron shock surfing acceleration. Astrophys. J. 572, 880–887.
Kasaba, Y., Bougeret, J.-L., Blomberg, L., Kojima, H., Yagitani, S., Moncuquet, M., Trotignon, J.-G., Chanteur, G., Kumamoto, A., Kasahara, Y., Omura, Y., Matsumoto, H., 2008. Plasma wave investigations (PWI) aboard the BepiColombo/MMO: first measurement of electric field, electromagnetic waves, and radio waves around Mercury. Planet. Space Sci. 56, 238–278.
Kokubun, S., Yamamoto, T., Acuna, M.H., Hayashi, K., Shiokawa, K., Kawano, H., 1994. The GEOTAIL magnetic field experiment. J. Geomagn. Geoelectr. 46, 7–21.
Lucek, E.A., Cargill, P., Dunlop, M.W., Kistler, L.M., Balogh, A., Baumjohann, W., Fornacon, K.-H., Georgescu, E., Haerendel, G., 2001. The magnetopause at ultra-high time resolution: structure and lower-hybrid waves. Geophys. Res. Lett. 28, 681–684.
Milillo, A., Fujimoto, M., Kallio, E., Kameda, S., Leblanc, F., Narita, Y., Cremonese, G., Laakso, H., Laurenza, M., Massetti, S., McKenna-Lawlor, S., Mura, A., Nakamura, R., Omura, Y., Rothery, D.A., Seki, K., Storini, M., Wurz, P., Baumjohann, W., Bunce, E., Kasaba, Y., Helbert, J., Sprague, A., 2008. The BepiColombo mission: an outstanding tool for investigating the Hermean environment. Planet. Space Sci. 56, 40–60.
Orsini, S., Livi, S., Torkar, K., Barabash, S., Milillo, A., Wurz, P., Di Lellis, A.M., Kallio, E., et al., 2008. SERENA: a suite of four instruments (ELENA, STROFIO, PICAM and MIPA) on board BepiColombo—MPO for particle detection in the Hermean Environment. Planet. Space Sci. 56, 166–181.
Othmer, C., Glassmeier, K.-H., Cramm, R., 1999. Concerning field line resonances in Mercury's magnetosphere. J. Geophys. Res. 104, 10369–10378.
Ness, N.F., Behannon, K.W., Lepping, R.P., et al., 1971. Use of two magnetometers for magnetic field measurements on a spacecraft. J. Geophys. Res. 76, 3565–3573.
Paschmann, G., Papamastorakis, I., Baumjohann, W., Sckopke, N., Carlson, C.W., Sonnerup, B.U.Ö., Lühr, H., 1986. The magnetopause for large magnetic shear: AMPTE/IRM observations. J. Geophys. Res. 91, 11099–11115.
Russell, C.T., 1989. ULF waves in the Mercury magnetosphere. Geophys. Res. Lett. 16, 1253–1256.
Saito, Y., Sauvaud, J.A., Hirahara, M., Barabash, S., Delcourt, D., Takashima, T., Asamura, K., et al., 2008. Scientific objectives and instrumentation of Mercury plasma particle experiment (MPPE) onboard MMO. Planet. Space Sci. 56, 182–200.
Siscoe, G.L., Ness, N.F., Yeates, C.M., 1975. Substorms on Mercury. J. Geophys. Res. 80, 4359–4363.
Slavin, J.A., Owen, C.J., Connerney, J.E.P., Christon, S.P., 1997. Mariner 10 observations of field-aligned currents at Mercury. Planet. Space Sci. 45, 133–141.
Smart, D.F., Shea, M.A., 1985. A simplified model of timing the arrival of solar flare-initiated shocks. J. Geophys. Res. 90, 183–190.
Suzuki, T.K., 2002. On the heating of the solar corona and the acceleration of the low-speed solar wind by acoustic waves generated in the corona. Astrophys. J. 578, 598–609.
Yamamoto, T., Matsuoka, A., 1998. PLANET-B magnetic fields investigation. Earth Planets Space 50, 189–194.
Zelenyi, L., Oka, M., Malova, H., Fujimoto, M., Delcourt, D., Baumjohann, W., 2007. Particle acceleration in Mercury's magnetosphere. Space Sci. Rev. 132, 593–609.
Zhang, T.L., Baumjohann, W., Delva, M., Auster, H.-U., Balogh, A., Russell, C.T., Barabash, S., Balikhin, M., Berghofer, G., Biernat, H.K., Lammer, H., Lichtenegger, H., Magnes, W., Nakamura, R., Penz, T., Schwingenschuh, K., Vörös, Z., Zambelli, W., Fornacon, K.-H., Glassmeier, K.-H., Richter, I., Carr, C., Kudela, K., Shi, J.K., Zhao, H., Motschmann, U., Lebreton, J.-P., 2006. Magnetic field investigation of the Venus plasma environment: expected new results from Venus express. Planet. Space Sci. 54, 1336–1343.
Zhang, T.L., Delva, M., Baumjohann, W., Auster, H.-U., Carr, C., Russell, C.T., Barabash, S., Balikhin, M., Kudela, K., Berghofer, G., Biernat, H.K., Lammer, H., Lichtenegger, H., Magnes, W., Nakamura, R., Schwingenschuh, K., Volwerk, M., Vörös, Z., Zambelli, W., Fornacon, K.-H., Glassmeier, K.-H., Richter, I., Balogh, A., Schwarzl, H., Pope, S.A., Shi, J.K., Wang, C., Motschmann, U., Lebreton, J.-P., 2007. Little or no solar wind enters Venus' atmosphere at solar minimum. Nature 450, 654–656.